Plasma etching of HfO2 at elevated temperatures in chlorine-based chemistry

M. Helot, Thierry Chevolleau, L. Vallier, O. Joubert, Elisabeth Blanquet, Alexander Pisch, P. Mangiagalli, T. Lill

Plasma etching of HfO_2 at elevated temperatures in chlorine-based chemistry

M. Hélot
STMicroelectronics, 850 rue Jean Monnet, 38926 Crolles Cedex, France

T. Chevolleau,[a] L. Vallier, and O. Joubert
Laboratoire des Technologies de la Microélectronique, CNRS, 17 rue des martyrs (CEA-LETI), 38054 Grenoble Cedex 09, France

E. Blanquet and A. Pisch
LTPCM/INPG-CNRS-UJF, 1130 rue de la piscine, 38402 Saint-Martin-d'Hères, France

P. Mangiagalli and T. Lill
Applied Materials, 974 E. Arques Ave. M/S 81334, Sunnyvale, California 94086

(Received 20 May 2005; accepted 10 October 2005; published 9 December 2005)

Plasma etching of HfO_2 at an elevated temperature is investigated in chlorine-based plasmas. Thermodynamic studies are performed in order to determine the most appropriate plasma chemistry. The theoretical calculations show that chlorocarbon gas chemistries (such as CCl_4 or Cl_2-CO) can result in the chemical etching of HfO_2 in the 425–625 K temperature range by forming volatile effluents such as $HfCl_4$ and CO_2. The etching of HfO_2 is first studied on blanket wafers in a high density Cl_2-CO plasma under low ion energy bombardment conditions (no bias power). Etch rates are presented and discussed with respect to the plasma parameters. The evolution of the etch rate as function of temperature follows an Arrhenius law indicating that the etching comes from chemical reactions. The etch rate of HfO_2 is about 110 Å/min at a temperature of 525 K with a selectivity towards SiO_2 of 15. x-ray photoelectron spectroscopy analyses (XPS) reveal that neither carbon nor chlorine is detected on the HfO_2 surface, whereas a chlorine-rich carbon layer is formed on top of the SiO_2 surface leading to the selectivity between HfO_2 and SiO_2. A drift of the HfO_2 etch process is observed according to the chamber walls conditioning due to chlorine-rich carbon coatings formed on the chamber walls in a Cl_2-CO plasma. To get a very reproducible HfO_2 etch process, the best conditioning strategy consists in cleaning the chamber walls with an O_2 plasma between each wafer. The etching of HfO_2 is also performed on patterned wafers using a conventional polysilicon gate. The first result show a slight HfO_2 foot at the bottom of the gate and the presence of hafnium oxide-based residues in the active areas. © *2006 American Vacuum Society.*
[DOI: 10.1116/1.2134707]

I. INTRODUCTION

With the constant downscaling of complementary metal-oxide-semiconductor (CMOS) devices, SiO_2 gate dielectric thickness is expected to be in the sub-nanometer range for the 45 and 32 nm technological nodes.[1] For an oxide thickness thinner than 1.0 nm, the gate dielectric will not maintain its insulating property due to a high leakage current induced by the direct tunneling effect.[2] Lowering this effect requires an increase of the gate dielectric thickness by using new dielectric material presenting a higher permittivity. Many materials have been already investigated such as Al_2O_3,[3] La_2O_3,[4] Ta_2O_5,[5] TiO_2,[6] HfO_2,[7–10] ZrO_2,[8] and Y_2O_3.[11] One of the main issues for the integration of these materials is the interface compatibility with silicon. The dielectric has to be thermodynamically stable with silicon in order to avoid a silicate or silicide interface during deposition or subsequent treatments. Recent studies have reported a silicate interface formation with Y_2O_3 and La_2O_3 and silicide interface formation with ZrO_2 deposition.[12,13] HfO_2 and Al_2O_3 present a better interface compatibility with silicon and poly-silicon.[2] Al_2O_3, which has a constant dielectric of about 10, is a short-term candidate whereas HfO_2, which exhibits a dielectric constant of about 20, is a promising candidate for the next integrated circuits (IC) generation.[14]

For high-*k* material integration, the etch process has to be revisited and developed to address integration issues such as the etch rate, the etch uniformity, and etch selectivity with respect to the SiO_2 interface layer without damaging the underlying silicon surface. Plasma etching is considered as a viable technique to etch away the dielectric material. The etching of materials such as Al_2O_3, ZrO_2, and Y_2O_3 has been already investigated but only a few studies have been carried out on the etching of HfO_2.[15–18] This work is dedicated to the etching of HfO_2 at high temperature (425–625 K) in an inductively coupled plasma (ICP). A thermodynamic study has been performed to point out the more promising chemistry among the usually adopted halogens precursors and best etching conditions (which lead to the maximum values of volatile etch by-products). Starting from the selected chemistry, we have investigated the effect of plasma conditions

[a]Electronic mail: chevolleauth@chartreuse.cea.fr

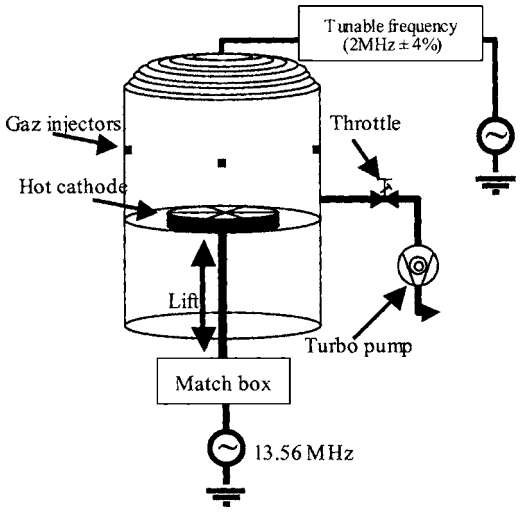

FIG. 1. Scheme of the DPS+ plasma reactor.

and chamber wall conditioning on the etch rate of HfO_2 and selectivity to the SiO_2 interface layer. Thanks to the diagnostics used, the evolution of the etch rate and selectivity will be discussed in terms of etching mechanisms and plasma surface interactions.

II. EXPERIMENTAL SETUP

Etching experiments have been carried out on 200 mm diameter wafers in a commercial high-density plasma-etching chamber (DPS+) made by Applied Materials, Inc. (Fig. 1). The DPS+ generates an inductively coupled plasma where both the source antenna and the bottom electrode are powered. The source consists of a ceramic dome with a three-dimensional coil configuration around it. The bottom electrode is powered at 13.56 MHz, and the source antenna at a tunable frequency (2 MHz with ±4%). The impedance matching with the bottom electrode generator is carried out by a classical radio-frequency (rf) match box whereas the matching with the source antenna generator is tuned by varying its frequency. The source power controls the ion density while the bottom electrode power controls the ion energy. The wafer sits on the bottom electrode and is clamped with an electrostatic chuck. The chuck temperature can be set from 425 to 625 K, and the temperature of the wafer is controlled by helium backside cooling at 2 Torr. Using separate heat exchangers, the chamber walls are held at 350 K and the ceramic dome at 330 K. The dome is air cooled when the plasma is on and is heated by infrared lamps when the plasma is idle. The chamber is pumped down by a turbo molecular pump providing a pumping speed of $1600\,l.s^{-1}$. The etching gases used in this study are Cl_2, CO, and O_2, and the pressure in the chamber is measured by a Baratron™ gauge and is regulated in a 4–100 mTorr range by a motorized throttle valve throughout the process.

For this study, thin HfO_2 and SiO_2 films of 10 nm have been deposited on 200 mm diameter silicon wafers by atomic layer deposition (ALD) and thermal oxidation, respectively. Before HfO_2 deposition, a pre cleaning and oxidation step of the Si wafer is required in order to obtain a good thermal interface compatibility between HfO_2 and silicon (as shown in Fig. 2). The etching of HfO_2 and SiO_2 has been investigated with Cl_2–CO gas chemistry. Pre- and post-partial etching thickness measurement of HfO_2 and SiO_2 films have been conducted with a spectroscopic UV-visible ellipsometer (Tencor SE 1280) in order to determine the etch rate.

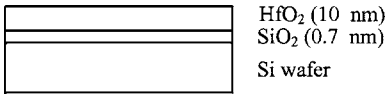

FIG. 2. Scheme of the HfO_2 wafers.

The etch cluster on which the DPS+ is mounted has been modified to host plasma and surface diagnostics. Additional ports have been added to the DPS+ with respect to its standard configuration. Using these additional ports, in-situ diagnostics such as spectroscopic UV-visible ellipsometry and mass spectrometry can be implemented on the DPS+ chamber. The ellipsometry is a very powerful technique to monitor the etching of thin films in real time.[19] The DPS+ source is also equipped with a powerful endpoint system, EyeD™ from Verity Instrument to allow real time monitoring of the etch process. This system combines two techniques: Interferometry and optical emission from the plasma. It is equipped with two optic fibers, one transporting the optical emission signal, and the other one the interferometry signal. Both signals can be acquired and observed simultaneously. Wavelengths from 200 to 800 nm can be monitored with this system, with an optical resolution of 1.7 nm. The optical emission mode is only available on the DPS+.

An x-ray photoelectron spectroscopy (XPS) surface analysis system (customized 220I system from VG scientific) is connected to the etch platform thanks to an additional transfer chamber connected to the cool down chamber of the cluster tool. After etching in the DPS+ plasma source, the wafer can be transferred under vacuum to the cool down chamber of the cluster tool and then into the additional transfer chamber. A detailed description of the XPS tool is given elsewhere.[20] The XPS measurements are performed with a nonmonochromatized x-ray source (Al $K\alpha$ at 1486.6 eV), at a constant dwelling time of 100 ms and at a constant pass energy (50 and 20 eV for the survey and core level spectra, respectively). The working distance between the sampled surface and the grounded entering part of the lens is around 2 cm. The angle between the optical axis of the input lens and the normal at the wafer is fixed at 45°. After partial etching, surface modifications of the remaining dielectric film are investigated by XPS. Chemical compositions are derived from the areas of the different XPS core level spectra. Spectral deconvolution is performed to extract the Hf4*f*, O1*s*, Si2*p*, C1*s*, and Cl2*p* peak intensities. Individual line shapes are simulated with the combination of Lorentzian and Gaussian functions using a commercial software package (ECLIPSE V3.1 Rev08). The background subtraction is performed by using a Shirley function. After XPS analysis, the

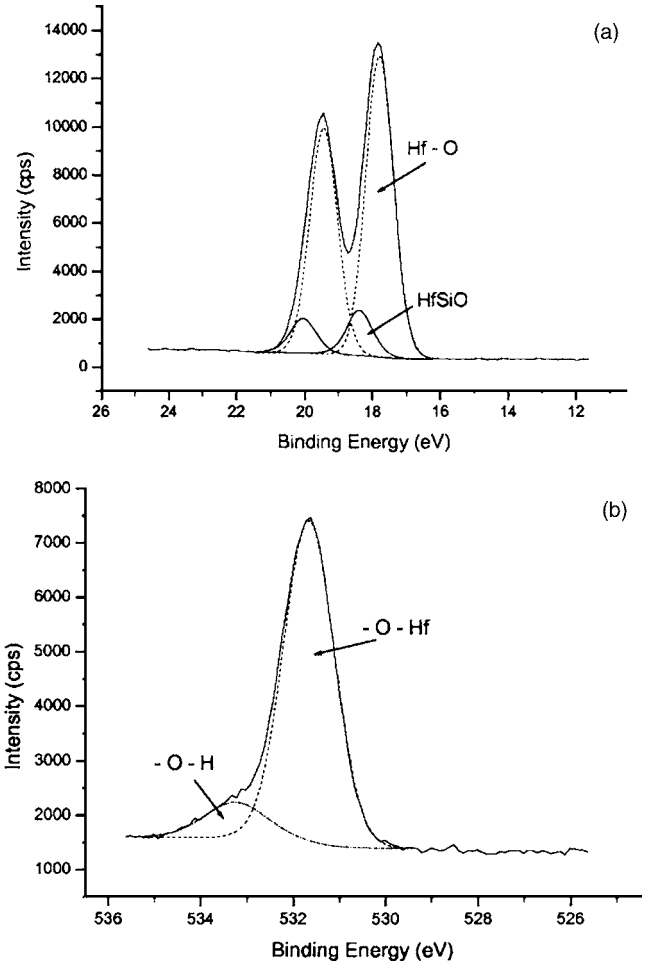

FIG. 3. XPS spectra of as deposited HfO_2; (a) Hf4*f*, (b) O1*s*.

integrated intensities are divided by the theoretical Scofield cross section (Hf4*f*:4.20;O1*s*:2.93;Si2*p*:0.82;C1*s*:1; Cl2*p*:1.51). The sum of the concentration of the different elements present on the analyzed surfaces is equal to 100%. Hydrogen content is not taken into account in this calculation since hydrogen cannot be detected by XPS. For the HfO_2 layer, the Hf4*f* core level spectra are fitted with a shift of 1.66 eV and intensity ratio of 0.75 for the spin-orbit Hf4*f* 7/2 and Hf4*f* 5/2.[21,22] For the as-deposited 10 nm thick HfO_2 film, the core level spectrum shows the presence of two Hf4*f* peaks. The main peak located at 17.6 eV is assigned to Hf–O bonds and the smaller contribution (only a few percent) at 18.2 eV can be attributed to Hf in a silicate (HfSiO) environment (Fig. 3). This second peak comes from the very thin silicate layer (about 0.5 nm) formed between the SiO_2 bottom interfacial layer and the HfO_2 film.[22] The O1*s* core level spectra reveal the presence of two peaks located at 533.3 and 531.6 eV, respectively. The main contribution at 531.6 eV is attributed to O bonded to Hf in a HfO_2 environment, and the smaller peak is assigned to OH bonds[23] (Fig. 3). The latter contribution is currently observed in an ALD deposition technique and such bonds are normally located on the near-top surface of the HfO_2 film.

In this work, we have also focused on the impact of chamber wall conditioning on the etch process. In a recent study, a new technique has been presented which allows determination by XPS the chemical nature and thickness of the layers deposited on the reactor walls during an etch process. The principle of the technique is to stick a small Al_2O_3 sample onto a 200 mm diameter silicon wafer with an air gap between the sample and the wafer in order to prevent RF biasing. Thus during the etch process, the Al_2O_3 sample experiences exactly the same plasma conditions as the Al_2O_3 chamber walls. As the sample is physically clamped on the wafer, it can be transferred under vacuum to the XPS chamber, allowing quasi *in situ* analyses of the deposited layers. More details of this technique are given elsewhere.[24]

III. RESULTS AND DISCUSSION

A. Thermodynamic study

For the etching of HfO_2, one of the main issues is the low volatility of halogenated-based etch by-products compared to the etching of SiO_2. Thermodynamic data shows that, at atmospheric pressure, Hf-based etch by-products ($HfCl_4, HfBr_4, HfF_4$) are less volatile than Si etch by products ($SiCl_4, SiBr_4, SiF_4$).[17] Of course, the products vapor pressures decrease at lower pressure. For the case of HfO_2 etching, the choice of the halogenated-based chemistry and substrate temperature are crucial parameters. In this work, thermodynamic studies have been carried out at our operating pressure (4 mTorr) and temperature range (425–625 K) in order to select the most appropriate gas mixture and temperature leading to the maximum amount of Hf and O-based volatile products. Based on thermodynamic calculations in a closed system, the HfO_2 etch rate can be estimated as a function of the chemistry and temperature by using the FACTSAGE™ Software.[25]

1. Principle of thermodynamic calculation

The FACTSAGE™ software calculates all the gaseous and condensed species existing in a closed system for a given substrate and gas mixture in thermodynamic equilibrium conditions at specified temperature and pressure. The calculation is based on the total Gibbs energy minimization of the system. A polynomial analytic function for the Gibbs free energy for each phase of the system (stable and metastable) is generated by a least squares optimization procedure from a coherent set of experimental information. These Gibbs energy data are stored in databases, and, for this study, the SGTE substance database has been used.[26] Based on this thermodynamic approach, we are able to determine an etch chemistry leading to volatile compounds and to estimate an etch rate under pure chemical etching conditions. The thermodynamic calculations do not simulate the real situation since on one hand a plasma is not a system in thermodynamic equilibrium conditions and on the other hand this thermodynamic approach does not take into account the ion bombardment of the plasma.

TABLE I. Thermodynamic and plasma etching studies for HfO_2 with various halogenated-based chemistries at 4 mTorr.

Atoms (gas mixture)	Thermodynamic results: Etching	Thermodynamic results: Gaseous species	Plasma etching (from 450 K)
$Cl(Cl_2)$	No	Cl_2, Cl	No
$Cl+O$ (Cl_2-O_2)	No	Cl_2, O_2, Cl	No
$Cl+C$ (CCl_4)	Yes from 400 K	$HfCl_4$, CO_2, CO, Cl_2	Not performed
$Cl+C+O$ (Cl_2-CO)	Yes from 400 K	$HfCl_4$, CO_2, CO, Cl_2	Yes
$Cl+H$ (HCl)	No	HCl	No

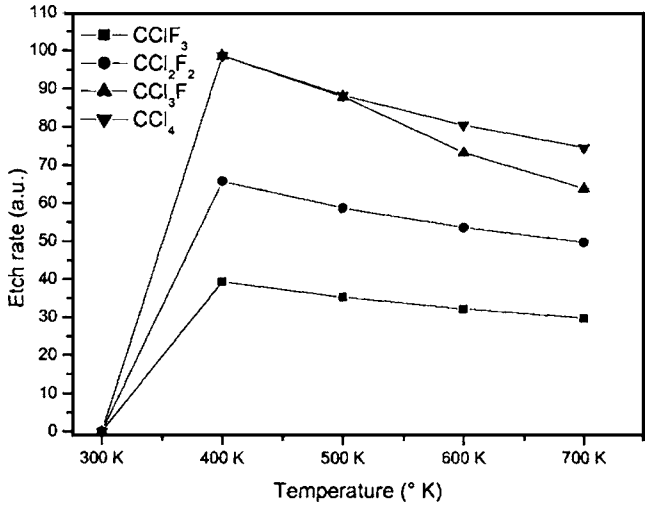

FIG. 4. Evolution of the thermodynamically calculated HfO_2 etch rate as a function of F-Cl ratio in CCl_xF_y based chemistries.

For example, let us consider the etching of HfO_2 in CCl_4 plasma at 400 K and 4 mTorr. In such a case, the thermodynamic system is composed of four elements Hf, O, C, and Cl. The thermodynamic calculation starts by considering CCl_4 (C and Cl atoms) with a large amount of HfO_2 in the solid phase. After minimization of the total Gibbs energy, the FACTSAGE software lists all possible gaseous and condensed species present in the closed system at thermodynamic equilibrium. The main gaseous species are CO_2 and $HfCl_4$ and the main condensed species are $HfCl_4$ on HfO_2 in the solid phase. There are other gaseous species such as CO, Cl_2, and Cl in low enough amounts that they can be neglected. These results show that carbon and chlorine containing chemistries can lead to the etching of HfO_2 by forming CO_2 and $HfCl_4$. The etch rate can be estimated from the calculation of the flow of each gaseous and condensed species under open conditions assuming molecular flow and the validity of the Hertz-Knudsen relation.[27]

2. Etching chemistries investigated

Based on the data given in the literature,[17] $HfCl_4$ is the halogenated compound which exhibits the lowest melting and boiling temperature at 1 atm. Firstly, we have investigated a wide variety of chorine-based chemistries in order to select the most appropriate gas mixture and temperature. Table I shows the thermodynamic results for the different chlorine-based chemistries investigated. The pressure has been chosen at 4 mTorr (working pressure in the DPS^+ chamber) and the temperature has been varied from 300 to 700 K. For comparison, the etching behavior obtained experimentally by plasma is also listed in Table I. The etching has been carried out in the DPS^+ chamber at the same pressure and gas flow ratio. No bias has been applied to the wafer in order to approach pure chemical etching conditions.

With a pure chlorine-based chemistry (Cl_2), thermodynamic calculations show that HfO_2 is not etched whatever the temperature, up to 700 K. The addition of oxygen (Cl_2-O_2) or hydrogen (HCl) does not lead to the etching of HfO_2 as shown in Table I. No condensed species is present on the HfO_2 surface with both chemistries which indicates that no chemical reactions occur on the surface in this temperature range (300–700 K). Experimentally, HfO_2 is not etched at 700 K under Cl_2 and Cl_2-O_2 plasma exposure which is in good agreement with the thermodynamic calculations. When using chlorocarbon-based chemistries (such as CCl_4), the thermodynamic calculation shows that HfO_2 etching proceeds at 400 K and the main gaseous species are CO_2, CO, and $HfCl_4$. These results indicate that chlorine and carbon lead to the chemical etching of HfO_2 by forming volatile etch effluents such as $HfCl_4$ and CO_2 at temperatures higher than 400 K. At lower temperature, there is no etching and condensed $HfCl_4$ is obtained with the remaining solid HfO_2. This reveals that $HfCl_4$ is nonvolatile under such conditions and consequently that etching does not occur. With chlorocarbon-based chemistries containing oxygen (such as Cl_2-CO), HfO_2 is etched at temperatures higher than 400 K with $HfCl_4$ and CO_2 as main etch effluents. The etch behavior predicted by thermodynamics is similar to a pure chlorocarbon-based chemistry which suggests that the addition of oxygen has a low impact on the chemical etch process. HfO_2 plasma etching experiments have been carried out successfully in Cl_2-CO plasma at 425 K which confirms the trends obtained from the thermodynamic study. When using chlorocarbon-based chemistry with fluorine addition (as CCl_xF_y), thermodynamic studies predict that the etching of HfO_2 proceeds from 400 K as shown in Fig. 4. In the temperature range investigated (300–700 K) at 4 mTorr the main etch effluents are CO_2 and $HfCl_4$ and HfF_4 is obtained as condensed species with the remaining HfO_2. At a temperature lower than 400 K, HfO_2 is not etched since both $HfCl_4$ and HfF_4 are not volatile and they are only present as condensed species with HfO_2. Figure 4 shows the evolution of the calculated HfO_2 etch rate as a function of temperature for different F-Cl ratios in CCl_xF_y-based chemistries. The etch rate is lower when the F–Cl ratio increases in the gas mixture at temperatures higher than 400 K. The decrease in the etch rate is explained by the non volatility of HfF_4 in the tempera-

TABLE II. HfO_2 and SiO_2 etch rate for two different bias in a Cl_2–CO plasma.

	HfO_2 etch rate	SiO_2 etch rate	Selectivity
0 W bias	110 Å/min	5 Å/min	20
25 W bias	155 Å/min	65 Å/min	2.5

ture range investigated. Indeed when the F–Cl ratio increases, a lower amount of reactive species (Cl atoms) leading to the formation of volatile by-products ($HfCl_4$) are present in the gas mixture which induces a slow down in the etch rate. Thermodynamic studies, therefore, predict that a chlorocarbon gas mixture (such as CCl_4) seems to be the most promising chemistry to etch HfO_2 under pure chemical etching conditions. Indeed such etch processes lead to formation of volatile effluents such as $HfCl_4$ and CO_2 at temperatures higher or equal to 400 K. The addition of fluorine in such chemistries (CCl_xF_y) slows down the etching since HfF_4 is not volatile in the temperature range investigated (300–700 K). However, CCl_4 has not been selected because of technical and safety reasons. In this work, we have chosen a Cl_2–CO plasma chemistry to study and characterize a promising HfO_2 etch process in the DPS^+ chamber.

B. Plasma etching in a Cl_2–CO chemistry

1. Etching mechanisms

Etching of HfO_2 and SiO_2 have been carried out in a Cl_2–CO (40/40 sccm) plasma chemistry without bias at a wafer temperature of 625 K, source power 800 W and 4 mTorr. Under these low ion energy plasma conditions, the etch rate of HfO_2 and silicon is about 110 Å/min whereas SiO_2 etching is negligible (etch rate lower than 10 Å/min). Because of these plasma conditions, a good selectivity between HfO_2 and SiO_2 is obtained (higher than 10), whereas a poor selectivity between HfO_2 and silicon is measured (about 1). When a low bias is applied to the wafer (25 W), the selectivity to SiO_2 decreases and is lower than 3 (as shown in Table II). Based on these results, the Cl_2–CO plasma chemistry without substrate bias becomes a very promising etch process since HfO_2 can be etched with a good selectivity towards SiO_2. After partial etching of a thin SiO_2 film under these conditions, the XPS survey revealed the presence of C and Cl indicating the formation of a chlorine-rich carbon overlayer on the SiO_2 surface. The C1*s* core level spectra can be fitted with three peaks (Fig. 5). The two main contributions at 286 and 286.9 eV can be assigned to C–C and C–Cl bonds, respectively. We assume that the third peak located at 288.9 eV which only represents a few percent can be attributed to C═O bonds since O is observed in very small concentrations (a few percent) in the CCl overlayer. The Cl2*p* core level spectra are fitted with a shift of 1.6 eV and an intensity ratio of 0.5 for the spin-orbit Cl2*p*3/2 and Cl2*p*1/2.[21] The Cl2*p* core level spectrum exhibits one peak located at 201 eV which is assigned to C–Cl bonds (Fig. 5). The chlorine-rich carbon overlayer formed on SiO_2 exhibits a C–Cl ratio of 1.3. After partial etching of the HfO_2 film, the

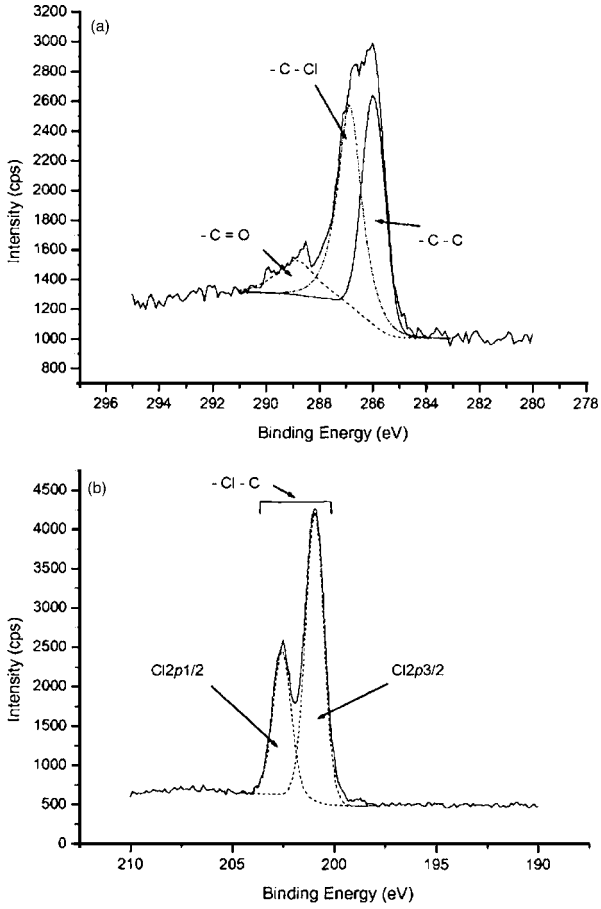

FIG. 5. C1*s* (a) and Cl2*p* (b) spectra after partial etching of the SiO_2 layer in a Cl_2–CO plasma.

XPS analyses reveal that neither C nor Cl is detected on the top of the HfO_2 surface. Thus the selectivity of HfO_2 towards SiO_2 is obtained because of the formation of the chlorine-rich carbon overlayer formed on SiO_2 during the etch process. This layer acts as a protective layer limiting the reactive species diffusion to the SiO_2 surface.

However, the experiments have shown that the HfO_2 etch rate under the conditions described previously is not reproducible. Indeed after screening several plasma parameters to optimize the process, the etch rate of HfO_2 using the baseline process is not always identical. In some cases, XPS analyses reveal the presence of a chlorine-rich carbon layer on the HfO_2 surface. It is well known that the coatings formed on the chamber walls by etch products and/or plasma species can generate etch process drifts and that chemical etching processes are very sensitive to the reactive neutral concentration in the plasma (which is strongly affected by their recombination rate on the chamber walls[28]). In the next section, we will investigate the impact of chamber wall coating on the etch process.

2. Impact of chamber walls coating on the etch process

We have used the simple technique described in Sec. II to monitor the coatings formed on the chamber wall during the

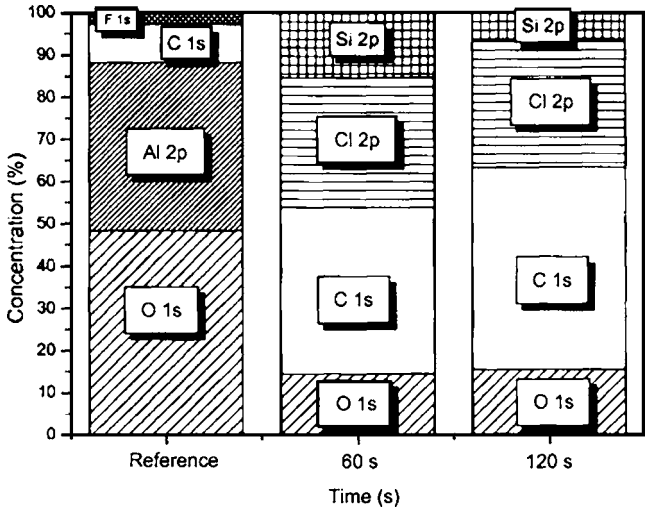

FIG. 6. Surface composition determined by XPS on the Al_2O_3 sample after different exposure times in a Cl_2-CO plasma.

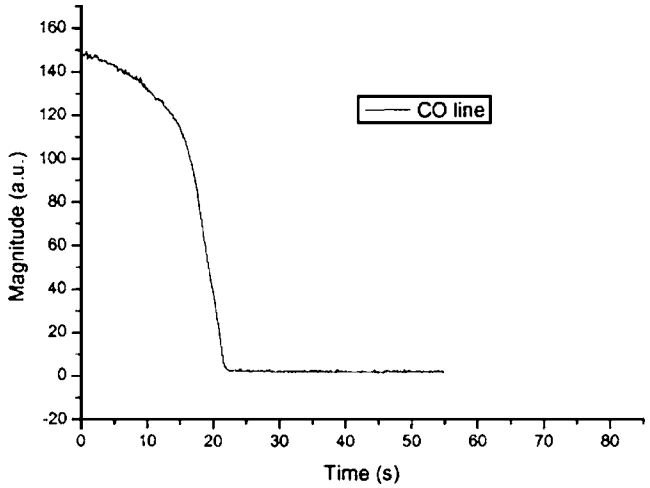

FIG. 7. Evolution of CO emission line in an O_2 plasma (cleaning step to remove the chlorine-rich carbon layer on chamber wall).

etch process. In this technique, a small Al_2O_3 sample is fixed onto the 200 mm diameter wafer with an air gap between the sample and the wafer in order to simulate a chamber wall surface.[24] The baseline etch process was carried out on a bare SiO_2 wafer with a small Al_2O_3 sample stuck on the wafer to analyze the coatings formed on the chamber walls using different etching times (Fig. 6). Prior to exposure to the plasma, the XPS analyses reveal the presence of a small concentration of carbon on the reference Al_2O_3 sample due to atmospheric surface contamination. Fluorine is also detected on the surface, originating from the residual fluorine present in the load lock chamber. After exposure to the Cl_2-CO plasma for two different times (60 and 120 s), XPS analyses shown in Fig. 6 demonstrate that the layer formed on the Al_2O_3 sample is mainly composed of C and Cl with a small fraction of Si and O (around 10%). No Al is detected in the layer probed by XPS demonstrating that the chlorine-rich carbon layer deposited on Al_2O_3 (i.e., on the chamber walls) during Cl_2-CO plasma etching of SiO_2 is thicker than the depth probed by XPS (approximately 10 nm). The C1*s* core level spectra exhibits the same shape as those observed on the SiO_2 surface, and it can be fitted with three peaks. The two main contributions at 286 and 286.9 eV can be assigned to C–C and C–Cl bonds, respectively. The third peak at 289.6 eV can be related to C═O bonds due to the presence of a small amount of O in the chlorine-rich carbon layer. The deconvolution of Cl2*p* core level spectra reveals the presence of one peak which is assigned to C–Cl bonds. The chlorine-rich carbon layer formed during the etch process on the Al_2O_3 sample, i.e., the chamber walls, exhibits a C–Cl ratio of 1.5 whatever the time of plasma exposure, indicating the growth of a homogeneous layer.

a. Plasma processes developed in clean chambers Based on the XPS analyses performed on the floating Al_2O_3 sample, we have shown that a chlorine-rich carbon layer is formed on the chamber wall during the etching of a SiO_2 wafer in a Cl_2-CO plasma. A simple O_2-based plasma has been developed to remove the chlorine-rich carbon layer from the chamber wall between each wafer. To monitor the chamber wall cleaning process, the CO emission line is recorded during the O_2 plasma. Figure 7 shows the evolution of the CO emission line recorded during the O_2 plasma used to clean the chamber wall previously coated by a chlorine-rich carbon layer. A sharp decrease of the emission line is observed after a few tens of seconds of O_2 plasma followed by a plateau which indicates that the chlorine rich carbon layer has been removed from the chamber wall. In addition, XPS analyses reveal that carbon and chlorine are not detected on the Al_2O_3 sample after the O_2 plasma. These results clearly show that the O_2 plasma is efficient to remove the deposited layer formed on the chamber wall during the Cl_2-CO etching process.

b. Chamber wall conditioning strategies In order to prevent repeatability issues and etch process drifts, two strategies have been investigated. In the first strategy, a clean process is performed first, followed by a 2 min Cl_2-CO plasma on a bare SiO_2 wafer used for the plasma chamber conditioning (generating the formation of a chlorine-rich carbon layer on the chamber walls). In the second strategy, the clean process is only performed without the conditioning step.

Figure 8 shows the etched thickness of HfO_2 as function of time using the Cl_2-CO baseline etch process when the first strategy is applied. The HfO_2 etched thickness is about 3 nm after 15 s and then remains constant, showing that the etching of HfO_2 has stopped. XPS analyses show the presence of carbon and chlorine on the HfO_2 surface after partial etching which indicates the formation of a chlorine-rich carbon layer on the HfO_2 surface. The C1*s* core level spectrum which exhibits the same shape as those observed on the SiO_2 surface can be fitted with three peaks at 286, 286.9, and 288.9 eV. These contributions are attributed to C–C, C–Cl, and C═O, respectively. The deconvolution of Cl2*p* core level spectrum shows not only the presence of C–Cl bonds located at 201 eV but also the formation of Hf–Cl bonds located at 199.6 eV.[18] These results indicate the formation of

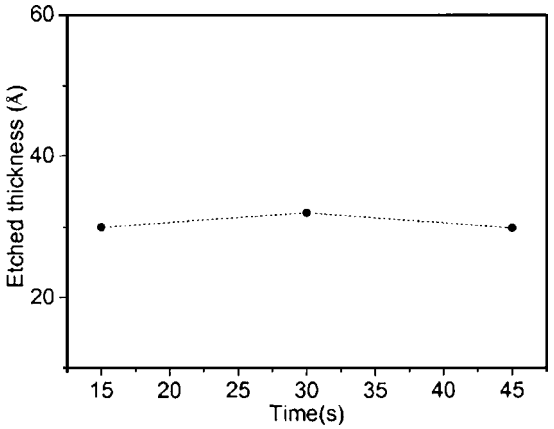

FIG. 8. Etched thickness of HfO_2 as function of the time in a Cl_2–CO plasma with the cleaning and conditioning step before etching (first conditioning strategy).

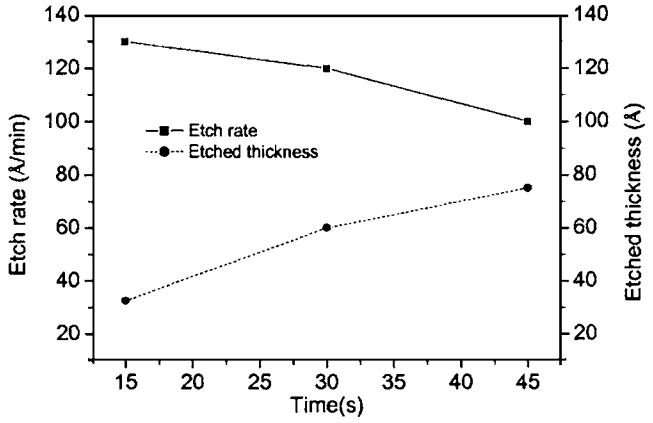

FIG. 10. Etched thickness and etch rate of HfO_2 as function of time in Cl_2–CO with the cleaning step before etching.

$HfCl_x$ interfacial layer between the HfO_2 film and the chlorine rich carbon layer. Figure 9 shows the surface composition determined by XPS after partial etching of HfO_2 for three different etching times. Carbon and chlorine concentrations increase with time whereas the Hf concentration decreases. These trends point out that the chlorine-rich carbon layer grows continuously during the etch process and that it is responsible for the etch stop phenomenon. From these experiments, we can conclude that the first strategy explained above (clean process followed by a conditioning step) is not appropriate since the HfO_2 etching proceeds only for a few seconds (less than 15 s) and then stops.

Figure 10 shows the etched thickness and etch rate as function of time with the baseline process using the second strategy (a clean process only prior to etching). The etched thickness increases with time indicating that the etching proceeds without etch stop. XPS analyses after partial etching show that no carbon and chlorine are detected on the HfO_2 surface. These results indicate that, in the absence of a chlorine rich carbon layer formation on the HfO_2 surface, the etching proceeds at a constant rate without etch stop. These results show that the strategy consisting of cleaning the chamber walls between each wafer generates reproducible HfO_2 etch rate in Cl_2–CO plasmas.

C. Influence of plasma parameters

In this section, we have investigated the impact of the temperature and plasma parameters (source power, Cl_2–CO ratio and pressure) on the HfO_2 etch rate and selectivity to SiO_2. Prior to HfO_2 etching, an O_2 plasma is performed in order to get reproducible etch process conditions as described in the previous section.

1. Influence of the cathode temperature

Figure 11 shows the evolution of the HfO_2 etch rate as function of the temperature with the Cl_2–CO baseline process (40 Cl_2, 40 CO, 4 mTorr, 800 W without bias power). The temperature investigated ranges between 425 and 625 K (425 K is the lowest temperature that can be achieved with the electrostatic chuck used in these experiments). The etch

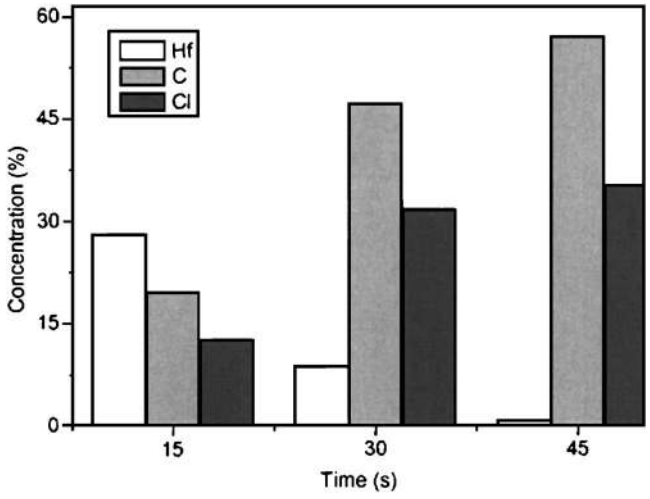

FIG. 9. Surface composition determined by XPS after partial etching of HfO_2 for three different etching times.

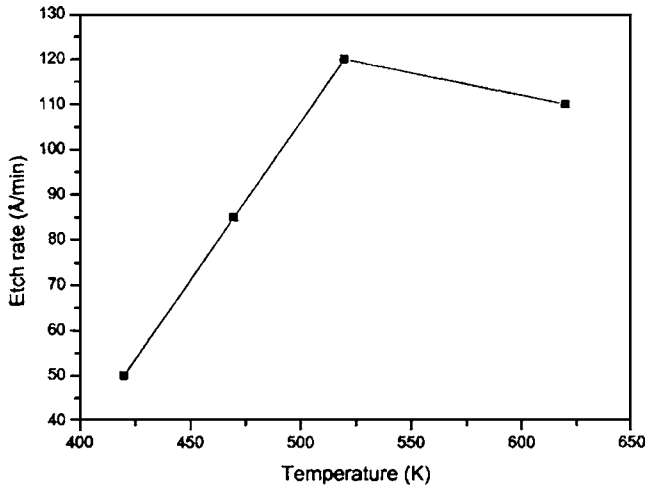

FIG. 11. Evolution of HfO_2 etch rate as function of the temperature with the Cl_2–CO baseline etch process.

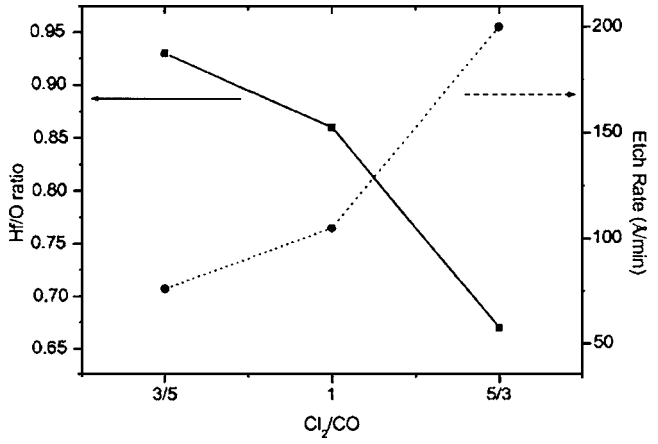

FIG. 12. Evolution of the HfO_2 etch rate as function of Cl_2-CO ratio without bias power applied to the wafer: HfO_2 etch rate (right axis) and Hf/O ratio (left axis).

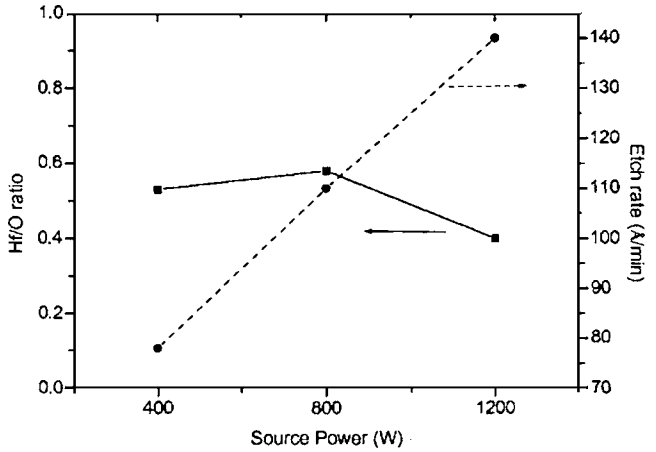

FIG. 13. Evolution of the HfO_2 etch rate as function of the source power without bias power applied to the wafer: HfO_2 etch rate (right axis) and Hf/O ratio (left axis).

rate increases as a function of the temperature (50 Å/min at 425 K) and reaches a plateau (120 Å/min) above 525 K. The evolution of the etch rate which follows an Arhenius law is similar to the evolution determined theoretically by the thermodynamic calculations (as shown in Figs. 4 and 11). This result indicates that the etching is mainly chemical. However, even in the absence of bias power applied to the wafer, it is bombarded by ions having an energy equal to the plasma potential (a few tens volts). The experimental results imply that the etch component assisted by the ion bombardment plays almost no role in the etching of HfO_2 at elevated temperatures. After partial etching, XPS analyses reveal that there is no carbon or chlorine on the HfO_2 surface regardless of the wafer temperature. These results indicate that, in the range investigated, the wafer temperature has no impact on the chlorine-rich carbon layer formation at the HfO_2 surface.

2. Impact of Cl_2-CO ratio on the etch performance

Figure 12 shows the etch rate evolution as function of the Cl_2-CO ratio injected in the plasma without bias power applied to the wafer. The pressure, source power and temperature have been set at 4 mTorr, 800 W, and 625 K, respectively. The HfO_2 etch rate increases with the chlorine concentration in the gas mixture from 50 to 200 Å/min when the Cl_2/CO ratio increases from 3/5 to 5/3, respectively. The SiO_2 etch rate is always lower than 10 $Å/min^{-1}$ for all the Cl_2-CO ratios investigated. By increasing the Cl_2-CO ratio, the HfO_2 to SiO_2 selectivity can be as high as 15.

XPS analyses reveal that no carbon or chlorine is detected on the HfO_2 surface, whereas a chlorine-rich carbon layer is formed on top of the SiO_2 surface leading to the selectivity between HfO_2 and SiO_2. XPS analyses also shows (see Fig. 12) that the HfO_2 surface becomes Hf-rich at low Cl_2-CO (3/5) ratio and reaches the stoichiometric Hf–O concentration at higher Cl_2-CO ratio (5/3). In this chemical etch process, Hf react with reactive chlorine species and O with carbon reactive species to form volatile $HfCl_4$ and CO_2 by products, respectively. When the Hf removal rate is lower than O removal rate (low Cl_2-CO ratio), the etching is limited by the reactive chlorine species leading to a slow down of the etch rate and to the formation of a hafnium-rich surface. However, when the Hf and O removal rate are the same (optimum Cl_2-CO ratio), the etch rate reaches a maximum and the HfO_2 surface remains stoichiometric in the steady state etching regime. Based on these results we can conclude that the Cl_2-CO ratio plays a key role in controlling the etch rate of HfO_2. In addition, a high selectivity to SiO_2 is achieved when the Cl_2-CO ratio is optimized to get the highest HfO_2 etch rate.

3. Impact of source power

Figure 13 shows the evolution of the etch rate of HfO_2 as function of the source power without bias applied to the wafer. The Cl_2-CO ratio has been set at 40/40 sscm and the pressure and temperature have been maintained at 4 mTorr and 575 K, respectively. The etch rate of HfO_2 increases linearly with the source power (up to 140 Å/min at 1200 W). XPS analyses reveal that no carbon or chlorine is detected on the HfO_2 surfaces and that the surface composition remains almost stoichiometric as a function of source power. The increase of the etch rate as a function of source power can be mainly attributed to a higher amount of chlorine and carbon reactive species reaching the HfO_2 surface when using higher source power. Contrary to HfO_2, the SiO_2 etch rate is hardly impacted whatever the source power used (etch rate lower than 10 Å/min in all the conditions analyzed). XPS analyses all show that a thick chlorine-rich carbon layer is formed on the top SiO_2 surface for all the source power investigated. Based on these results, we can conclude that an increase of the source power leads to higher HfO_2 etch rate and better selectivity to SiO_2.

4. Impact of pressure

Figure 14 shows the HfO_2 and SiO_2 etch rates as function of the pressure without bias power applied to the wafer. The

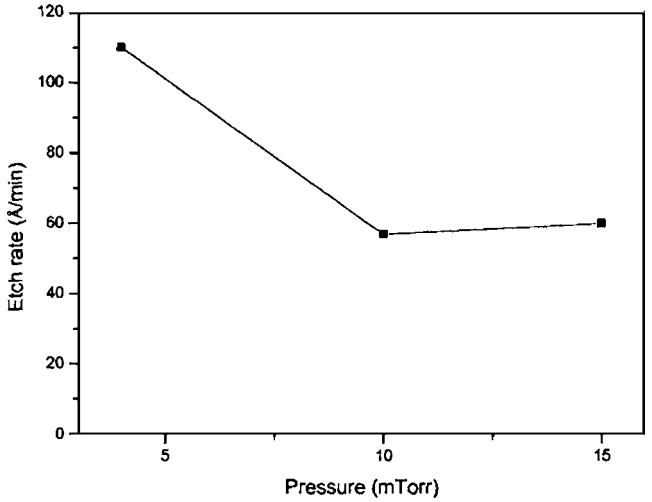

FIG. 14. Etch rate of HfO_2 and SiO_2 as function of the pressure without bias power applied to the wafer.

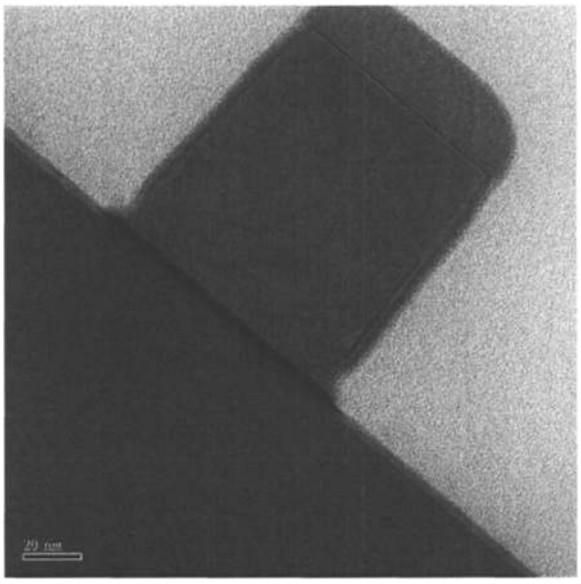

FIG. 15. TEM cross section of a 50 nm isolated line after full gate stack etching and HfO_2 removal.

Cl_2–CO ratio has been set at 40/40 sscm and the source power and temperature have been kept at 800 W and 575 K, respectively. The HfO_2 etch rate decreases from 110 to 60 Å/min when the pressure increases from 4 to 15 mTorr. A better uniformity is achieved at low pressure (<10 mTorr). XPS analyses reveal that there is no chlorine rich carbon layer formed on top of the HfO_2 surface whatever the pressure. This result indicates that lower etch rate observed with an increase of the pressure is not attributed to an etch stop phenomenon but rather to a slow down of the etching. This can be attributed to less carbon and chlorine reactive species present in the gas phase at higher pressure leading to lower Hf and O removal rate.

SiO_2 etch rate is hardly etched whatever the pressure with an etch rate lower than 10 Å/min. XPS analyses reveal that the low etch rate is attributed to the formation of chlorine-rich carbon layer for all the pressure investigated. However, the thickness and composition of the chlorine-rich carbon layer change with the pressure. The thickness decreases with an increase of the pressure with an overlayer less rich in carbon.

D. Patterned wafers

In order to study the integration of HfO_2 as a gate oxide, HfO_2 etching has been performed on patterned wafers using a typical polysilicon gate stack. The wafers have been patterned with direct write electron-beam lithography, resulting in small dimensions (down to 50 nm in isolated lines and 75 nm in dense lines). The stack is composed of 3.5 nm HfO_2, 100 nm lightly doped poly-Si, 40 nm SiO_2 (used as hard mask) and 210 nm Sumitomo chemical resist. The hard mask opening step, ashing and gate etch process have been carried out in a DPS etcher which is connected to the same cluster tool as the DPS^+. The DPS generates an inductively coupled plasma where both the source antenna and the bottom electrode are powered. The chuck temperature is set at 325 K, the chamber walls are held at 350 K and the ceramic dome at 330 K. More details are given elsewhere.[29] A typical process has been used to etch the 50 nm thick SiO_2 hard mask via a fluorocarbon plasma. After ashing of the remaining resist mask, the polysilicon gate has been etched to the HfO_2 underlayer with a three step etch process. The main etch step ($HBr–Cl_2–O_2$) ensures the etching of three-quarter of the silicon thickness and is followed by the soft landing step ($HBr–Cl_2–O_2$ with less aggressive ion bombardment conditions) which is launched about 10 nm before reaching the HfO_2 gate oxide layer. Finally, the overetch step ($HBr–O_2$) finishes the silicon etching.

Based on the results presented in the previous section, the 3.5 nm thick HfO_2 layer has been etched using the following process conditions: 40 Cl_2, 40 CO, 4 mTorr, 800 W without bias at 625 K. This etch process provides a high HfO_2 etch rate and a better uniformity. The selectivity toward SiO_2 is

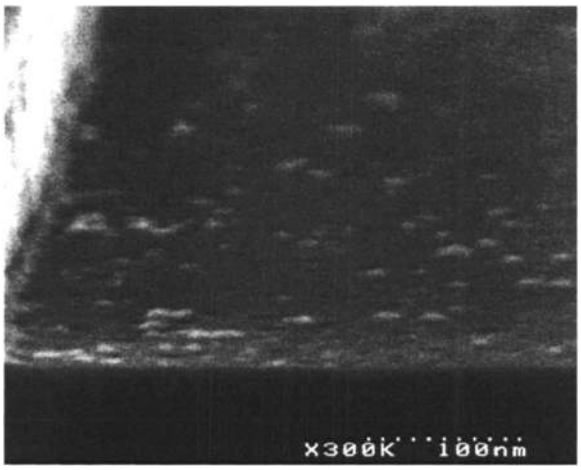

FIG. 16. Cross-sectional SEM picture of a polysilicon gate showing the Si bulk surface (active areas).

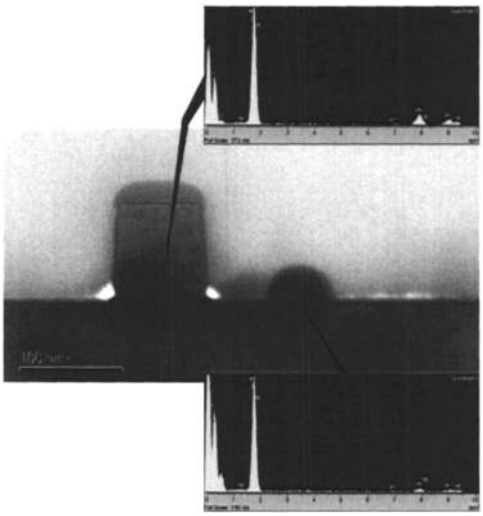

FIG. 17. EDX measurements of an isolated polysilicon gate after full gate etch stack and HfO_2 removal.

higher than 15 which allows a control of the etch process by time. Figure 15 shows the transmission electron microscopy (TEM) cross section picture of a 50 nm isolated line after full gate stack etching and HfO_2 removal. The polysilicon gate features exhibit straight profiles with a slight notch at the bottom of the gate. A foot of HfO_2 is also observed at the bottom of the gate. No lateral etching of the polysilicon gate is generated during the HfO_2 removal step although this chemical etch process is not selective toward silicon (as previously shown in the previous section). This is explained by the SiOCl-based passivation layers formed during the gate etch process[30] which protect the polysilicon sidewalls. TEM picture confirm this explanation since the passivation layers are still present after the HfO_2 removal step. However no passivation layer is remaining at the bottom of the gate which is correlated to the presence of a notch. The notch formation can be attributed to a passivation layer which is not thick enough to protect the bottom of the polysilicon gate during all the HfO_2 etch process. It is well known that the passivation layer formed on the sidewalls during polysilicon gate etching is thinner at the bottom than at the top of the gate due to lower plasma exposure time. The TEM picture also reveals a very low underlying bulk silicon recess of about 1.5 nm. Because the HfO_2 etch process is selective to SiO_2, the etching has stopped on the interfacial SiO_2 layer. In such a case, the silicon recess can be explained by an oxidation of the bulk silicon when the interfacial SiO_2 layer is exposed to the Cl_2-CO plasma. Previous studies have already shown such oxidation phenomenon through very thin SiO_2 gate oxides during the etching of a polysilicon gate.[31] These studies have highlighted that the oxygen species present in the plasma diffuse through the thin SiO_2 layer leading to an oxidation of the Si bulk. Figure 16 shows a cross sectional SEM picture of the silicon surface after HfO_2 etching. A rough surface is observed with the presence of residues (like small dots) everywhere on the SiO_2 interfacial layer. XPS analyses reveals that these residues are hafnium oxide (HfO_x) which is also confirmed by a EDX (energy dispersive x-ray spectrometry) measurement as shown in Fig. 17. This result indicates that the residues come from the hafnium oxide which is locally not completely etched at the interface with the SiO_2 layer. This etching nonuniformity can be explained by a locally inhomogeneous HfO_2 layer in terms of density, cristallinity and chemical composition. Further surface analyses using local probe such as AFM are now mandatory to get a better understanding of the local nonhomogeneity of HfO_2.

The first results obtained on patterned wafers shows that a Cl_2-CO plasma without bias applied to the wafers is a promising process to remove the HfO_2 layer. However, improvements of such a chemical etch process are required in order to minimize the polysilicon notch and the HfO_2 foot at the bottom of the gate. In addition, the main issue with this process is to find a solution to remove the hafnium-based residues remaining after the etching. Our next paper, under preparation, will address this issue and will present a revisited etch process allowing the complete removal of HfO_2 residues.

IV. CONCLUSIONS

Cl_2-CO plasma chemistry has been investigated to etch HfO_2 at elevated wafer temperatures. Theoretical thermodynamic studies have shown that chlorocarbon gas chemistries (such as CCl_4 or Cl_2-CO) etch HfO_2 by forming volatile etch effluents such as $HfCl_4$ and CO_2 at temperatures higher or equal to 400 K. The thermodynamic studies have also underlined that HfF_4 is not volatile in a temperature range between 300 and 700 K which leads to a slow down of the etch rate when fluorine is added to a chlorocarbon gas mixture.

Experimentally, the HfO_2 etching proceeds in a Cl_2-CO plasma at a wafer temperature of 400 K. A good selectivity of HfO_2 towards SiO_2 (higher than 10) is achieved without bias applied to the wafer. The selectivity is obtained due to the formation of a chlorine-rich carbon overlayer formed on SiO_2 during the etch process. Under these low ion energy plasma conditions, the etching is mainly chemical and thereby the etch rate follows an Arhenius law. The Cl_2-CO ratio plays a key role in controlling the etch rate of HfO_2. The etch rate reaches a maximum at an optimum Cl_2-CO ratio with a HfO_2 surface remainining stoichiometric in the steady state etching regime.

A chlorine-rich carbon layer coating is formed on the chamber wall in a Cl_2-CO plasma. An O_2 plasma efficiently removes this deposited layer formed on the chamber walls. A drift of the HfO_2 etch process has been observed according to the chamber wall conditions (such as etch stop phenomenon). To get a reproducible HfO_2 etch rate without etch stop in Cl_2-CO plasmas, the best conditioning strategy consists in cleaning the chamber walls with an O_2 plasma between each wafer.

[1]International Technology Roadmap for Semiconductors, 2004 Update.
[2]G. D. Wilk, R. M. Wallace, and J. M. Anthony, J. Appl. Phys. **89**, 5243 (2001).

[3]L. Manchada *et al.*, Tech. Dig. - Int. Electron Devices Meet. 605 (1998).
[4]S. Ohmi, C. Kobayashi, L. Kashiwagi, C. Ohshima, H. Ishiwara, and H. Iwai, J. Electrochem. Soc. **150**, F134 (2003).
[5]C. Chaneliere, J. L. Autran, J. P. Reynard, J. Michailos, K. Barla, A. Hiroe, K. Shimonura, and A. Kakimoto, MRS Symposium Proceedings, 592, pp. 75–80 (2000).
[6]B. He, T. Ma, S. A. Campbell, and W. L. Gladfelter, Tech. Dig. - Int. Electron Devices Meet. 1038 (1998).
[7]M. Balog, M. Schieber, S. Patai, and M. Michman, J. Cryst. Growth **17**, 298 (1972).
[8]J. C. Lee, Microelectronics Research Center, The University of Texas at Austin 4th Annual Topical Research Conference on Reliability, 30 October (2000).
[9]Y. Kim *et al.* International Sematech, IEEE (2001).
[10]M. Yang, E. P. Gusev, M. Ieong, O. Gluschenkov, D. C. Boyd, K. K. Chan, P. M. Kozlowski, C. P. D'Emic, R. M. Sicina, P. C. Jamison, and A. I. Chou, IEEE Electron Device Lett. **24** (2003).
[11]V. Ioannou-Sougleridis, G. Vellianitis, and A. Dimoulas, J. Appl. Phys. **93**, 3982 (2003).
[12]C. Durand, C. Vallee, C. Dubourdieu, E. Gautier, M. Bonvalot, and O. Joubert, J. Vac. Sci. Technol. A **22**, 2490 (2004).
[13]Y. S. Lin, R. Puthenkovilakam, J. P. Chang, C. Bouldin, I. Levin, N. V. Nguyen, J. Ehrstein, Y. Sun, P. Pianetta, T. Conard, W. Vandervorst, V. Venturo, and S. Selbrede, J. Appl. Phys. **93**, 5945 (2003).
[14]B. H. Lee, L. Kang, W. J. Qi, R. Nieh, Y. Jeon, K. Onishi, and J. C. Lee, IEDM Tech. Digest 133–136 (1999).
[15]S. Norasetthekul, P. Y. Park, K. H. Baik, K. P. Lee, J. H. Shin, B. S. Jeong, V. Shishodia, D. P. Norton, and S. J. Pearton, Appl. Surf. Sci. **187**, 75 (2002).
[16]L. Sha and J. P. Chang, J. Vac. Sci. Technol. A **22**, 88 (2004).
[17]J. Chen, W. J. Yoo, Z. YL. Tan, Y. Wang, and D. S. H. Chan, J. Vac. Sci. Technol. A **22**, 1552 (2004).
[18]L. Sha, R. Puthenkovilakam, Y.-S. Lin, and J. P. Chang, J. Vac. Sci. Technol. B **21**, 2420 (2003).
[19]S. Vallon, O. Joubert, L. Vallier, F. Ferrieu, B. Drévillon, and N. Blayo, J. Vac. Sci. Technol. A **15**, 865 (1997).
[20]E. Pargon, O. Joubert, N. Posseme, and L. Vallier, J. Vac. Sci. Technol. B **22**, 1858 (2004).
[21]J. F. Moulder *et al.*, *Handbook of X-ray Photoelectron Spectroscopy*, edited by J. Chastain (Perkin-Elmer, Eden Prairie, 1992).
[22]O. Renault, D. Samour, J.-F. Damlencourt, D. Blin, F. Martin, S. Marthon, N. T. Barret, and P. Besson, Appl. Phys. Lett. **81**, 3627 (2002).
[23]J.-F. Damlencourt, O. Renault, D. Samour, A.-M. Papon, C. Leroux, F. Martin, S. Marthon, M.-N. Séméria, and X. Garros, Solid-State Electron. **47**, 1613 (2003).
[24]O. Joubert, G. Cunge, B. Pelissier,L. Vallier, M. Kogelschatz, and E. Pargon, J. Vac. Sci. Technol. A **22**, 553 (2004).
[25]C. W. Bale, P. Chartrand, S. A. Degterov, G. Eriksson, K. Hack, R. Ben Mahfoud, J. Melan, A. D. Pelton, and S. Petersen, FACTSAGE thermochemical software and database Calphad, 26(2) (2002) 189–228.
[26]http://www.sgte.org/ substance database V. 10
[27]L. Dumas, C. Chatillon, and E. Quesnel, J. Cryst. Growth **222**, 215 (2001).
[28]G. Cunge, R. L. Inglebert, O. Joubert, L. Vallier, and N. Sadeghi, J. Vac. Sci. Technol. B **20**, 2137 (2002).
[29]X. Detter, R. Palla, I. Thomas-Boutherin, E. Pargon, G. Cunge, O. Joubert, and L. Vallier, J. Vac. Sci. Technol. B **21**, 2174 (2003).
[30]F. H. Bell, and J. Joubert, J. Vac. Sci. Technol. B **15**, 88 (1997).
[31]L. Desvoivres, L. Vallier, and O. Joubert, J. Vac. Sci. Technol. B **18**, 156 (1999).